Journal of
Materials Chemistry C

Accepted Manuscript

Journal Name

RSCPublishing

ARTICLE

Defect Rich Seed Mediated Growth: A Novel Synthesis Method to Enhance Defect Emission in Nanocrystals

Cite this: DOI: 10.1039/xoxxoooooox

Received ooth January 2012,
Accepted ooth January 2012

DOI: 10.1039/xoxxoooooox

www.rsc.org/

Adersh Asok,[a] A. R. Kulkarni*[b] and Mayuri N. Gandhi[a]

In the present work, we show the synthesis of defect rich ZnO quantum dots (QDs) of different sizes by considering both thermodynamic and kinetic principles. Initially, defect rich smaller size ZnO QDs are prepared by spontaneous nucleation and crystallization of ZnO under different dielectric heating rate. We observed an enhanced defect emission in ZnO QDs synthesized at rapid heating rate when compared with ZnO QDs synthesized at slow heating rate. This implies a thermodynamic incorporation of high density of defects in ZnO QDs. These QDs are then used as a seed for the growth of different size defect rich ZnO QDs. The photoluminescence study confirms that the QDs grown from defect rich seed shows increased defect emission in comparison with QDs grown from seeds with fewer defects. All the different size QDs grown from defect rich seed exhibits high quantum yield, good stability, monodispersity and possess size tunable defect emission. The demonstrated synthesis approach is a promising strategy to enhance defect emission in nanocrystals.

Introduction

Native defect engineering in perfectly ordered semiconductor crystals are immensely important, as it imparts novel physical properties to the material, without the addition of external impurities. At nanoscale these native defects are predominant at the surface of the nanocrystals (NCs)[1-5] and it plays a major role in endowing novel functionalities, including defect induced optical absorption, carrier trapping, catalysis, luminescence, magnetism and electrical properties.[6-14] The most recent results on both theoretical and experimental work reports that defect density increases with decreasing NCs size.[1,4] This increase in defect density is due to the increase of surface to volume ratio of smaller NCs, where majority of the atoms are on the surface leading to a range of degrees of coordination to form strained lattice. As a result of this strained lattice, surface defects are generated. This modifies the intrinsic interatomic distances and alters the energy levels of bonding electron, resulting in the modifications in electronic and optical properties of NCs.[15]

This modification in energy levels associated to surface defects can be either beneficial or detrimental, depending on the semiconductor compositions. In most of the semiconductor compositions, surface defects are acting as fast non-radiative de-excitation channels for photogenerated charge carriers, thereby reducing the fluorescence quantum yield (Q.Y.) of band edge emission (BEE).[16] In the case of most metal oxide semiconductors these surface defects are responsible for radiative transitions, resulting in a broad defect emission (DE) band at the expense of BEE.[2,3,17,18,19]

Among metal oxide semiconductors, ZnO is of more technological importance due to its, direct band gap (Eg = 3.37 eV), large exciton binding energy (60 meV) and rich defect chemistry.[19,20] The presence of native defects in ZnO results in a broad DE, which allows a semi-quantitative analysis of defect density in ZnO by comparing DE with its BEE. This qualifies ZnO a perfect material choice to study defect chemistry at nanoscale. Recently the defect rich ZnO (D-ZnO) quantum dots have attracted more attention due to the modifications of energy levels induced by native defects. These defect energy levels along with quantum size effect can be used to obtain tunable visible emission in the entire visible spectrum without any impurity doping.[3,5,21,22] Hence, promoting native surface defects in ZnO quantum dots (QDs) is highly desirable, for making highly luminescent, cheap and non-toxic alternative to toxic heavy metal based QDs. Moreover, defect induced properties in ZnO QDs are attracting many potential applications in solar energy absorption, photoelectrochemical water splitting, catalysis, sensors, in vitro and in vivo diagnostics, nanomedicine to name a few.[23-27]

In the context of many potential applications, numerous publications have focused on the synthesis of D-ZnO NCs. Most of these reports concentrate on synthesis environment, physical methods, rapid hydrolyzes of Zn salt, stoichiometry and doping for defect promotion in ZnO NCs.[5,9,21-23,27-30]

Journal Name

RSCPublishing

ARTICLE

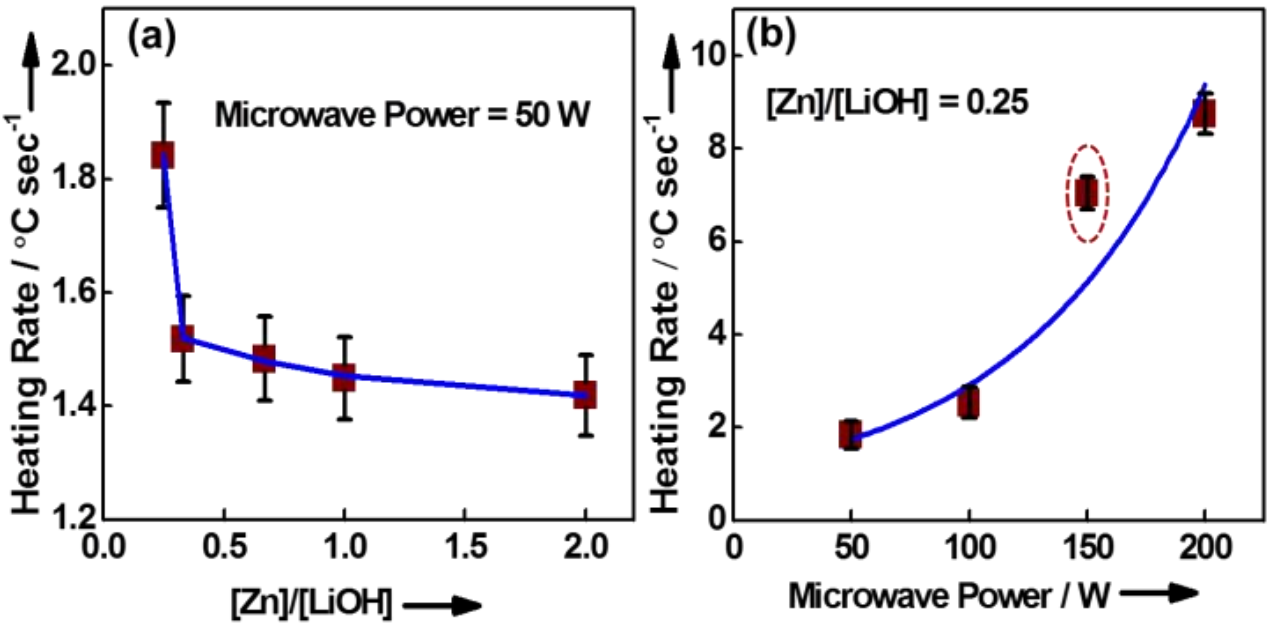

Fig. 1 a) The microwave heating profile for different concentration of LiOH at a microwave power of 50W (refer, Fig. S1 for reaction profile), b) The microwave heating profile for [Zn]/[LiOH] = 0.25 at different microwave power (refer, Fig. S2 for reaction profile), the data point inside the dotted oval represents the optimum heating rate.

To the best of our knowledge there is no report on promoting defects in variable size ZnO QDs by combining both thermodynamic and kinetic approach. In this study we have combined both these approaches for the synthesis of variable size D-ZnO QDs. Initially we synthesized defect rich ZnO seed QDs by making use of thermodynamic approach. In order to thermodynamically promote defects in the seed QDs, rapid crystallization of ZnO at a higher temperature is an essential prerequisite.[9,31] Here, we hypothesize that ultra-fast heating of reaction mixture well above the crystallization temperature of ZnO will result in the spontaneous crystallization of ZnO QDs. This spontaneous process creates a non-equilibrium condition which contributes toward an increase in entropic terms, resulting in the incorporation of high density of defects in the crystals.

Results and discussion

Defect enrichment by rapid microwave heating

Microwave based rapid dielectric heating was adopted to test this hypothesis, as it allows rapid and uniform heating of reaction mixture by dipolar polarization and ionic conduction.[32,33] In this work, a highly polar solvent ethanol was used as solvent matrix for achieving high heating rate by dipolar polarization.[34] In order to achieve rapid heating of the reaction mixture; we used ionic conduction mechanism of microwave heating as the first step. It was found that an increase in concentration of LiOH adds up to an increase in heating rate of reaction mixture (Fig. 1a), and a maximum heating rate was achieved for [Zn]/[LiOH] = 0.25 at a microwave power of 50 W.

In the next step further improvement in heating rate was achieved by increasing microwave power during synthesis. The heating rate was found to increase with microwave power (Fig. 1b). It was observed that at high microwave power (200 W) the heating rate of solution was very high, which could not be controlled effectively. This resulted in overheating of reaction mixture well beyond the set temperature range of 75±5°C (Fig. S2). The ZnO QDs formed above the set temperature were found to precipitate out due to poor colloidal stability. Since, the stability of QDs in the synthesis solution is needed for practical applications; we have limited the microwave power to

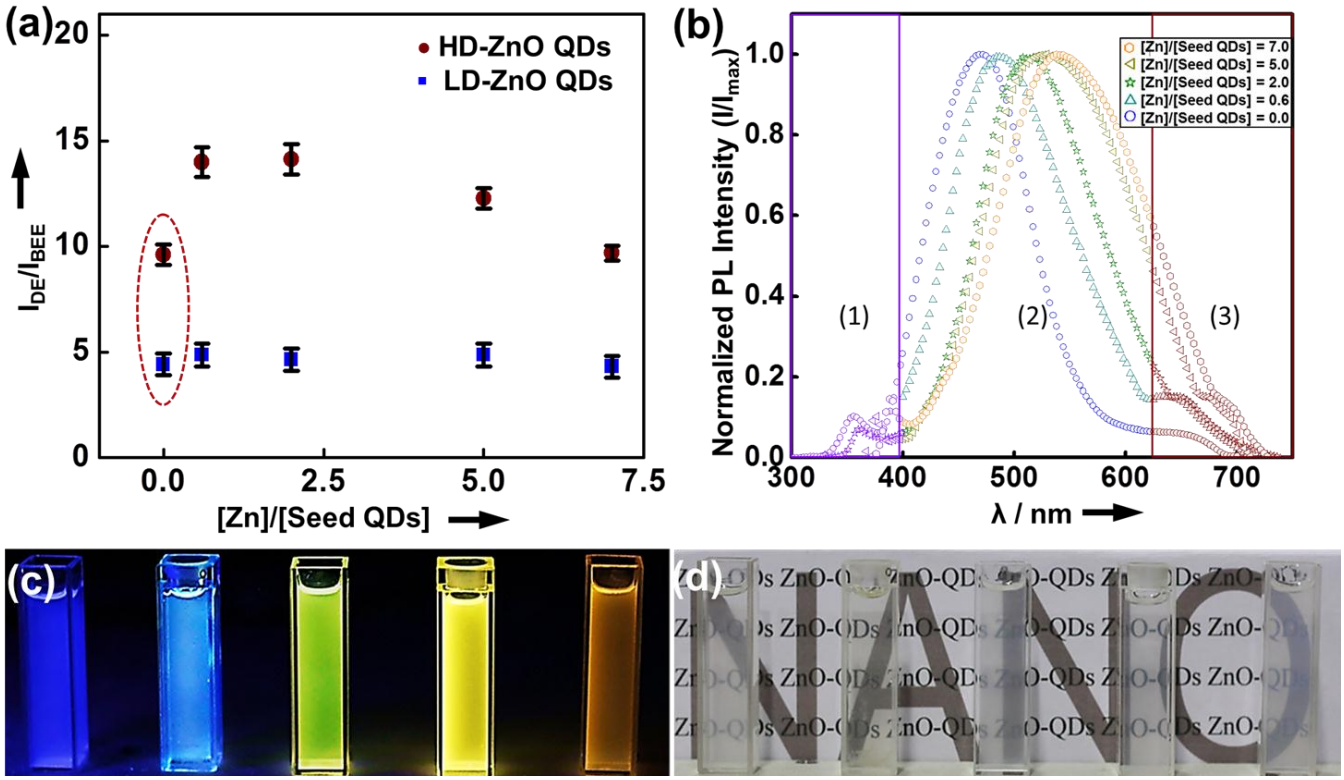

Fig. 2 a) The I_{DE}/I_{BEE} value for QDs of different size grown from S_{HD}-ZnO QDs and S_{LD}-ZnO QDs, the data points in the dotted oval represent the I_{DE}/I_{BEE} value for seed QDs.b) Normalized PL(I/I_{max}) emission spectra of different size D-ZnO QDs grown from S_{HD}-ZnO QDs and S_{HD}-ZnO QDs. c) Photographs of dilute ethanolic solutions of S_{HD}-ZnO QDs and other different size QDs grown from it under 365 nm (4W) UV irradiation, d) and under room light.

150 W. At this power a good control of temperature was achieved along with a fast heating rate of ~7°C/ sec. In order to check the thermodynamic promotion of defects in seed ZnO QDs, two different seed QDs (size ~2.92±0.2 nm) synthesized at two different heating rates (~1.8°C/sec (50 W) and ~7°C/sec (150 W)) were studied using photoluminescence (PL) spectroscopy. The ratio of the intensity of λ_{max} of defect emission (I_{DE}) to λ_{max} of UV emission (I_{BEE}) could be used to describe semi-quantitatively the defect density in ZnO QDs.[35,36] The PL spectra of QDs synthesized at two different heating rates were normalized with respect to I_{BEE}. The results showed that I_{DE}/I_{BEE} ratio of QDs synthesized at ~7°C/sec was higher compared with those synthesized at ~1.8°C/sec (Fig. 2a and Fig. S3). This clearly suggests that rapid microwave heating induce a high density of defects in ZnO QDs. We have labelled seed QDs synthesized at a heating rate ~1.8°C/sec as seeds with less defect density (S_{LD}-ZnO QDs) and synthesized at rapid heating rate ~7°C/sec as seed with high defect density (S_{HD}-ZnO QDs).

Seed Mediated Growth of Different Size D-ZnO QDs

Gas chromatography coupled to mass spectrometry (GC−MS) was performed for the investigation of organic by-products formed during the synthesis of seed ZnO QDs. From the Gas chromatogram and mass spectra (Fig. 3b), it is evident that acetate molecules undergoes esterification reaction with ethyl alcohol, which resulted in the formation of ethyl acetate. In order to initiate esterification reaction a protonating agent is required. Here the possible protonating agent is Li^+ ions; therefore it takes part in the esterification reaction by reducing back to LiOH, establishing a catalytic role for LiOH. This represents the chemical basis for the generation of the ZnO quantum dots; overall reaction scheme is given in Fig. 3a. It was observed that smaller QDs of size ~ 2.96 nm was formed at

Journal Name

RSCPublishing

ARTICLE

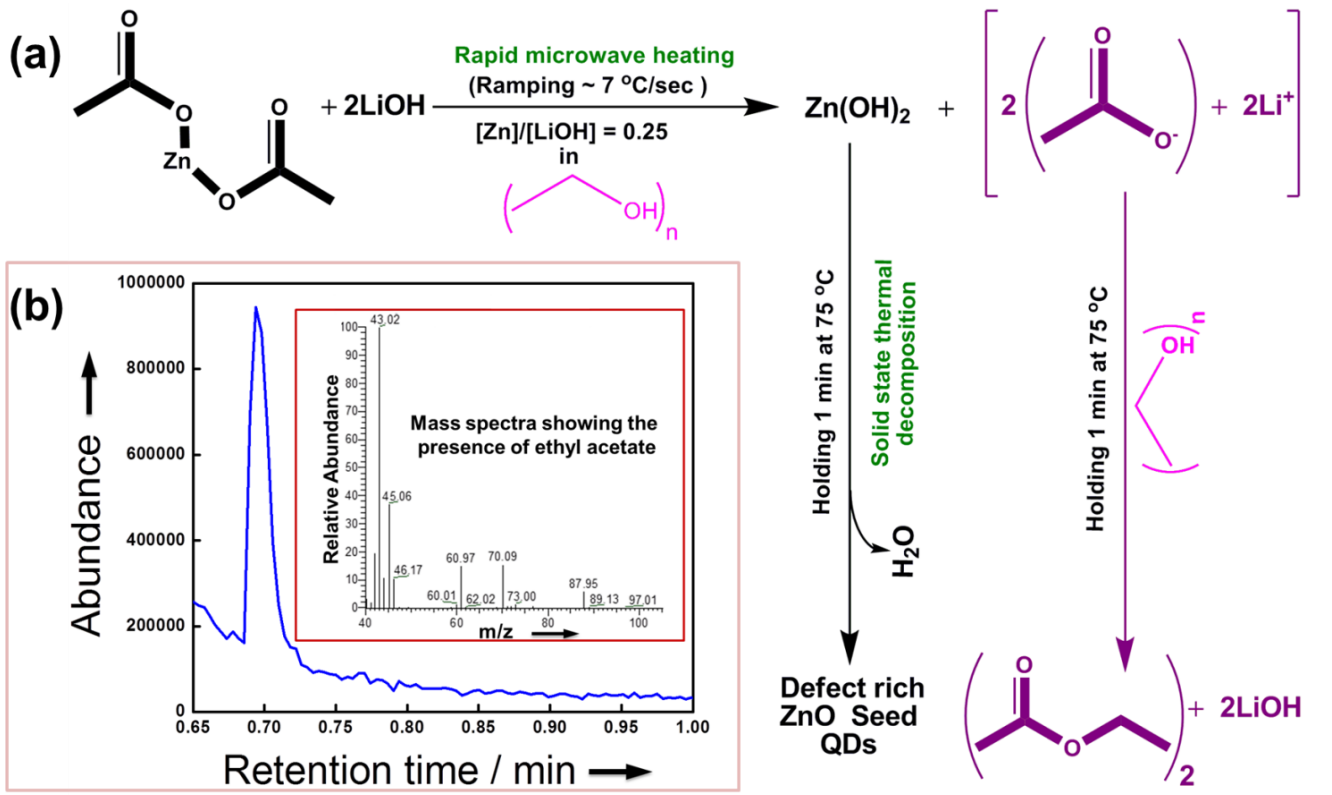

Fig. 3 a) The reaction scheme for the synthesis of defect rich ZnO seed QDs by microwave chemistry, b) Gas chromatogram of the net organic reaction product with elution peak at 0.69 min corresponding to ethyl acetate, corresponding mass spectrometry data is given as inset.

[Zn]/[LiOH] = 0.25 due to counter ion capping. This is beneficial; since the size reduction makes the vacancy much easier to form[1,4] at the same time we can use this as seed QDs for the growth of larger QDs. The growth was achieved by adding zinc acetate to the D-ZnO seed QDs and different particle size was obtained by controlling the [Zn]/[Seed QDs] ratio. The seed mediated growth was performed in S_{LD}-ZnO and S_{HD}-ZnO QDs. The I_{DE}/I_{BEE} ratios of both sets are given in Fig. 2a.

It was found that the different size QDs grown from S_{HD}-ZnO QDs have a higher I_{DE}/I_{BEE} when compared with that grown from S_{LD}-ZnO QDs. This suggests that the defect propagation from seed QDs to the other different size QDs grown from that seed. Therefore, it can be concluded that the defect density of seed QDs determine the defect density of other different size QDs grown from that seed.

PL Characterization of Defects and Quantum Size Effect

The normalized PL spectra (I/I_{max}) of S_{HD}-ZnO QDs and other different size QDs grown from it are shown in Fig. 2b. The broad PL spectra can be divided up into three regions: 1) emission from band edge.[35,36] 2) emission centered at visible range, from oxygen vacancy (V_o)[3,37,38,39] and 3) near infrared (NIR) emission from zinc vacancy V_{zn}.[40] It may be noted that with increasing QD size, all these emission peaks showed a bathochromic shift, which was attributed to a quantum confinement effect in different size QDs. A similar trend was followed by the photoluminescence excitation (PLE) spectra (Fig. S5) of QDs, which confirmed that the defect emissions of QDs were subjected to quantum size effect. This size dependent shift in PL signifies that S_{HD}-ZnO QDs can act as nucleation centers and grow by the reduction of zinc ions at their surfaces. The broadening of PLE spectra was also observed when QDs size decreases. This is due to its increased surface defect density when compared with defect rich QDs of larger size. As

a result of this large amount of lattice disorder occurs in the smaller ZnO QDs and this could yield several mid-gap states. The presence of this mid-gap states resulted in the extended energy state called band tail states. This is reflected as board PLE spectra for smaller QDs, because this will act as a dominant optical excitation and relaxation centers.[41] Figure 2c shows a photograph of highly luminescent D-ZnO QDs emitting a different color with varying QD sizes under 365 nm (4 watt) UV lamp excitation and Figure 2d shows that the prepared D-ZnO QDs form a transparent and stable colloidal suspension in ethanol under room light.

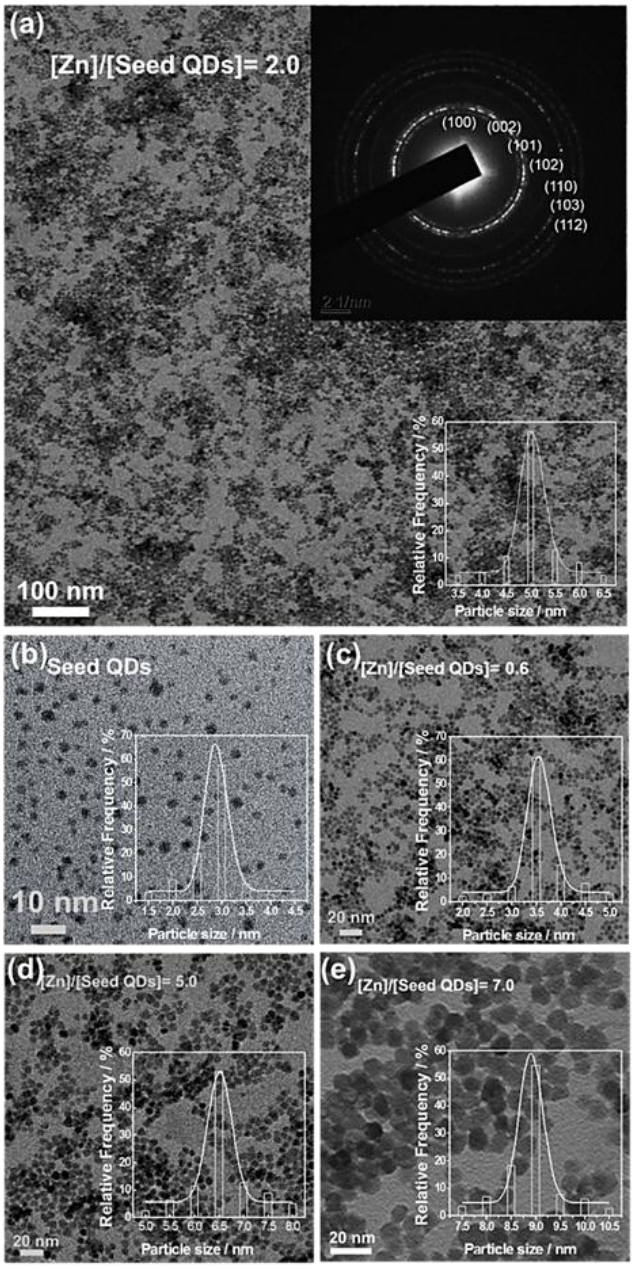

Fig. 4 TEM images of different sizes D-ZnO QDs grown from S_{HD}-ZnO QDs, a)TEM images and electron diffraction pattern (upper right inset) of the ZnO QDs prepared with [Zn]/[Seed QDs] = 2.0 b) S_{HD}-ZnO QDs c)[Zn]/[Seed QDs] = 0.6 c) d) [Zn]/[Seed QDs] = 5.0 and e) [Zn]/[Seed QDs] = 7.0

Size, Structural and Defect Characterization

All the different size D-ZnO QDs prepared by seed mediated growth from S_{HD}-ZnO QDs were further characterized for phase and purity by X-ray diffraction (XRD) and selected area electron diffraction (SAED) studies (Fig. S4 and Fig. 4a, upper right inset). The SAED pattern (Fig. 4a, upper right inset) shows seven diffuse diffraction rings from planes of wurtzite ZnO, which can be indexed as the (100), (002), (101), (102), (110), (103), and (112), starting from the inner to the outer ring, respectively. These studies confirm that QDs prepared possess wurtzite crystal structure of ZnO (JCPDS card No. 36-1451) without any impurity peaks. The broadening in XRD peaks and diffuse diffraction rings in SAED were observed. The broadening observed in X-ray diffraction peaks may be due to strained lattice or size effect. The observed diffuse diffraction rings can be attributed to coherent diffraction by strained surface of partially crystalline D-ZnO QDs.

The D-ZnO QDs synthesized by seed mediated growth were nearly spherical and showed good monodispersity, which was confirmed by analysing electron micrograph (Fig. 4). Particle size distribution profile (Fig. 4, bottom right insets) of different size D-ZnO QDs grown from S_{HD}-ZnO QDs shows a narrow size distribution for all different [Zn]/[Seed QDs] ratios.

This further affirms that size tuning of D-ZnO QDs can be achieved by varying the ratio of seed to metal ions, this resulted in size tunable emission along with high Q.Y., as shown in Table 1.

Table 1. Property comparison of D-ZnO QDs grown from S_{LD}-ZnO and S_{HD}-ZnO QDs.

[Zn]/[Seed QDs] ratio	size[a] (±0.2 nm)	excitation peak[b] (eV)	emission peak[c] (eV)	Q.Y.[d] (grown from S_{LD}-ZnO QDs)	Q.Y.[e] (grown from S_{HD}-ZnO QDs)
0.0	2.92	3.98	2.63	0.24	0.47
0.6	3.76	3.78	2.55	0.26	0.65
2.0	5.12	3.59	2.44	0.25	0.69
5.0	6.82	3.52	2.35	0.24	0.57
7.0	8.96	3.45	2.30	0.25	0.48

[a]Calculated using an approximation[42], [b]Measured from PLE spectrum (Fig. S5), [c]Measured from PL spectrum (Fig. 2b), [d, e]Q.Y. data (Fig. S6).

The high resolution transmission electron microscopy (HR-TEM) investigations were done to further probe the nature of D-ZnO QDs surface. Typical HR-TEM images of S_{HD}-ZnO QDs are shown in Fig. 5a, which show a high density of dark spots in the images along with strained lattice. We categorized the observed dark spots in HR-TEM as vacancy defects.[43] These vacancy defects contribute towards lattice strain in S_{HD}-ZnO QDs, as observed in HR-TEM image. The presence of these strained lattices contributes in the formation several closely spaced defect energy levels. This is evident from the broad and intense defect emission band of S_{HD}-ZnO QDs.

Journal Name RSCPublishing

ARTICLE

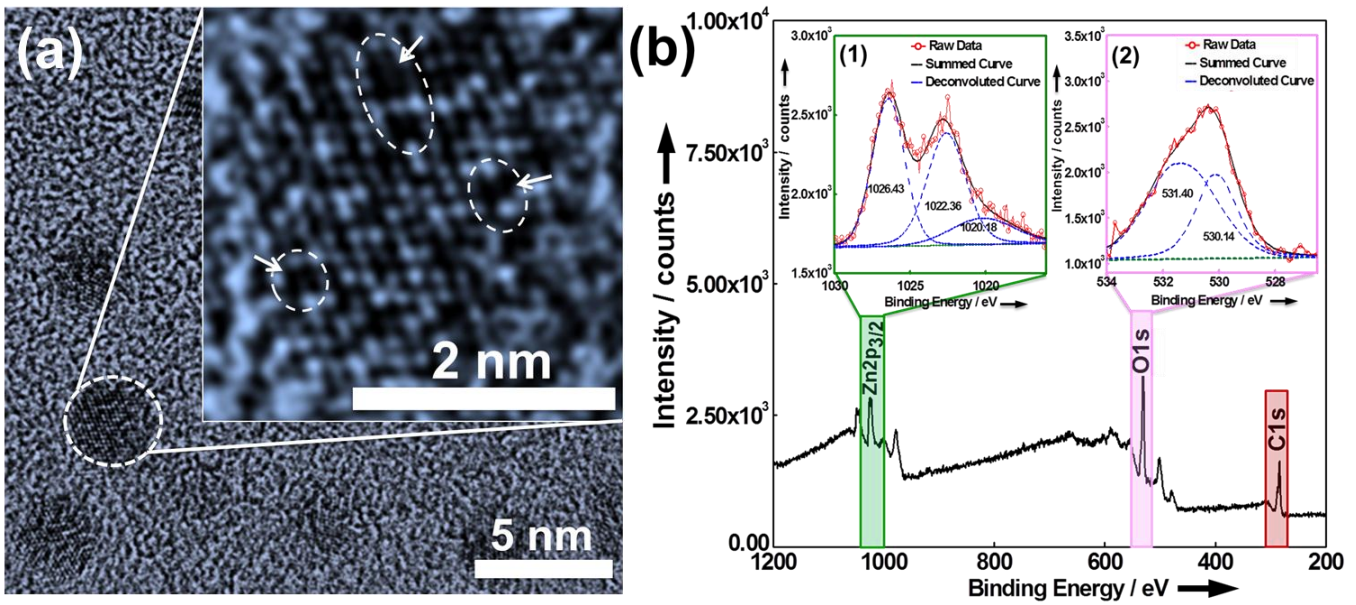

Fig. 5. a) HR-TEM image of S_{HD}-ZnO QDs synthesized at dielectric heating rate ~7°C/ sec, the inset shows the magnified image of one QD showing high density of defects(the arrow is a guide for eye). b) The XPS survey spectra of S_{HD}-ZnO QDs showing the chemical states of $Znp_{3/2}$ and O1s, the inset (1) and (2) shows the high resolution XPS spectra of the $Znp_{3/2}$ and O1s core levels.

In the next step we studied the nature of defects formed in S_{HD}-ZnO QDs as a result of rapid dielectric heating. To study the chemical state of defects, X-ray photoelectron spectroscopy (XPS) was done. The XPS survey spectra and high resolution spectra of $Zn2p_{3/2}$ and O1s for S_{HD}-ZnO QDs are shown in Fig. 5b. The binding energy of Zn2p and O1s peaks were calibrated by taking C1s peak at 284.6 eV as the standard peak (NIST standard reference database 20, Version 4.1.). The high resolution spectra for $Zn2p_{3/2}$ and O1s shows broad peaks with ZnO related peaks at 1022.36 and 530.14 eV, respectively, and these values agree with the standard NIST XPS database for ZnO. The deconvoluted high resolution spectra for $Zn2p_{3/2}$ and O1s are shown as inset Fig. 5b(1) and Fig. 5b(2).

The result shows that the binding energy of $Zn2p_{3/2}$ peak has shifted to lower energy side when compared with the standard NIST peak for ZnO. The presence of this lower binding energy peak indicates a change in the chemical state of zinc, which can be accounted physically as the loss in number of oxygen atoms in S_{HD}-ZnO QDs.[44] Similarly a medium binding energy peak for O1s was observed at 531.40 eV, corresponds to the oxygen defects in the metal oxide matrix.[45] In case of $Zn2p_{3/2}$ peak, a clear splitting of peak to the higher binding energy (1026.43 eV) side was observed; this may be due to the presence of V_{zn}.[46] This XPS observation of V_{zn} is supported by the presence of NIR emission in the PL emission spectra.[40] This suggests that the observed broad PL emission from D-ZnO QDs was due to vacancies of both zinc and oxygen atoms at the surface. The PL spectroscopy studies strongly suggest that these vacancies are preserved and propagated to other different size D-ZnO QDs during seed mediated growth.

Conclusions

In summary, this synthesis approach results in size tunable, stable and monodispersed D-ZnO QDs within a few minutes. The S_{HD}-ZnO QDs were prepared by rapid dielectric heating shows increased defect emission. This S_{HD}-ZnO QDs were used as a seed for the growth of other different size D-ZnO QDs. The PL study confirmed that the QDs grown from S_{HD}-ZnO QDs show enhanced defect emission in comparison with QDs grown from S_{LD}-ZnO QDs. This verifies that defect density of seed QDs determine the defect density of other different size QDs grown from it. The underlying principles of this synthesis approach can be used for the synthesis of other different size defect rich nanocrystals.

Experimental Section

Chemicals

All reagents used for synthesis are commercially available. The solvent used for synthesis was absolute ethanol (Analytical

Reagent, China, Assay: 99.99 %). The raw precursors $Zn(OAc)_2$ (Sigma Aldrich, 99.99 %, metal basis) and LiOH (Sigma Aldrich, ≥ 98%, reagent grade) were used as received without further purification.

Preparation of Stock Solutions

Stock solutions are prepared in degassed absolute ethanol. The $Zn(OAc)_2$ stock solution consist of 0.05 M $Zn(OAc)_2$, prepared by dissolution of $Zn(OAc)_2$ via ultra-sonic mixing along with refluxing under N_2 atmosphere to obtain a clear solution. The LiOH stock solution consists of 0.2 M LiOH, prepared by ultrasonic mixing of LiOH powder in ethanol for 1 hour.

Synthesis of D-ZnO Seed QDs

In a typical synthesis 3 mL of $Zn(OAc)_2$ (0.05 M) was mixed with 3 mL of LiOH (0.2 M) in a 10 mL test tube kept below 0^oC to prevent the reaction during mixing. Then the test tube was sealed by using a polymer cap. The reaction was initiated by microwave irradiation with magnetic stirring, by using CEM Discover microwave reactor with operating frequency of 2.45 GHz. During a typical run, the microwave power (here, initial power was varied to achieve fast heating rate) was adjusted to heat the sample up to 75 ± 5^oC, and then the temperature was maintained for one minute with high magnetic stirring. The microwave radiation was switched off after one minute. Reaction mixture was quenched to room temperature by cooled compressed air flow. The ZnO QDs solution obtained was labelled as D-ZnO seed QDs of metal concentration 0.05 M.

Seed Mediated Growth of D-ZnO QDs

The D-ZnO seed QDs were diluted to Zn metal concentration of 0.01 M by ethanol, to this different concentration of metal precursors ($Zn(OAc)_2$ were added. The growth was initiated under microwave dielectric heating till 50^oC and maintained at one minute with magnetic stirring to obtain defect rich QDs of different size.

Characterization

Gas chromatography linked to mass spectrometry (GC-MS) was carried out on Thermo TR-5MS SQC, Trace GC-Ultra instrument equipped with a 15 m × 0.25 mm ×0.25 µm column. The carrier gas used was Helium at a flow rate of 1 $mLmin^{-1}$ and split ratio 1:50. The temperature of oven was maintained isothermally at 40^oC for 5 min, and then increased at a rate of 10^oC/min from 40 to 100^oC. The mass spectrum was acquired at a scan rate of 2.5 scans/s over the m/z range of 10−500. Transmission electron microscopy (TEM), high resolution TEM (HR-TEM), and selected area electron diffraction (SAED) were recorded using JEOL JEM-2100F high-resolution transmission electron microscope operating at 200 kV. X-ray photoelectron spectra were studied using a Thermofisher-VG Scientific (Multilab 2000) photoelectron spectrometer equipped with 150 W monochromatic Al Kα X-ray source. Curve-fitting was carried out using nonlinear (shirley-type) least-square fitting with software (XPS-PEAK 41) to separate the overlapping peaks. X-ray powder diffraction (XRD) data were collected using Philips (PANalytical) powder diffractometer PW3040/60 X'pert Pro with Cu Kα radiation. The photoluminescence (PL) spectra were acquired using HORIBA JobinYvon Fluorolog 3 model (quinine sulfate and rhodamine 6G were used as standard references for Q.Y. measurement).

Acknowledgements

We express our thanks to SAIF, IIT Bombay for GC-MS, HR-TEM studies and Department of Physics, IIT Bombay for XPS studies.

Notes and references

[a]*Centre for Research in Nanotechnology and Science, Indian Institute of Technology Bombay, Mumbai 400076, India.*
[b]*Department of Metallurgical Engineering and Materials Science, Indian Institute of Technology Bombay, Mumbai 400076, India.*
*Corresponding Author: Prof. A. R. Kulkarni,
Department of Metallurgical and Materials Science Engineering
Indian Institute of Technology Bombay, Mumbai 400076, India.
phone number: + 91-22-25767636
fax number: + 91-22-2572-3480
E-mail: ajit.kulkarni@iitb.ac.in

† Electronic Supplementary Information (ESI) available: Typical reaction profile, XRD patterns, PL spectra, PLE spectra and quantum yield are included. See DOI: 10.1039/b000000x/

1. M. Hegde, T. Wang, Z. L. Miskovic, P. V. Radovanovic, Appl. Phys. Lett. 2012, 100, 141903.
2. A. Kar, S. Kundu, A. Patra, J. Phys. Chem. C 2010, 115, 118-124.
3. L. Zhang, L. Yin, C. Wang, N. lun, Y. Qi, D. Xiang, J. Phys. Chem. C 2010, 114, 9651-9658.
4. G. Guisbiers, J. Phys. Chem. C 2011, 115, 2616-2621.
5. A. Asok, M. N. Gandhi, A.R. Kulkarni, Nanoscale 2012, 4, 4943-4946.
6. X. Chen, L. Liu, Y. Y. Peter, S. S. Mao, Science 2011, 331, 746-750.
7. A. Naldoni, M. Allieta, S. Santangelo, M. Marelli, F. Fabbri, S. Cappelli, C. L. Bianchi, R. Psaro, V. Dal Santo, J. Am. Chem. Soc. 2012, 134, 7600-7603.
8. S. Zander, E. L. Kunkes, M. E. Schuster, J. Schumann, G. Weinberg, D. Teschner, N. Jacobsen, R. Schlögl, M. Behrens, Angew. Chem., Int. Ed. 2013, 52, 6536-6540.
9. H. Zeng, G. Duan, Y. Li, S. Yang, X. Xu, W. Cai, Adv. Funct. Mater. 2010, 20, 561-572.
10. M. M. Krause, J. Mooney, P. Kambhampati, ACS Nano 2013, 7, 5922-5929.
11. W. H. Green, K. P. Le, J. Grey, T. T. Au, M. J. Sailor, Science 1997, 276, 1826-1828.
12. X. Xu, C. Xu, J. Dai, J. Hu, F. Li, S. Zhang, J. Phys. Chem. C 2012, 116, 8813-8818.
13. M. Venkatesan, C. B. Fitzgerald, J. M. D. Coey, Nature 2004, 430, 630-630.
14. A. M. Stoneham, Theory of Defects in Solids: Electronic Structure of Defects in Insulators and Semiconductor, Oxford University Press, USA, 2001.
15. G. Ouyang, W. G. Zhu, C. Q. Sun, Z. M. Zhu, S. Z. Liao, Phys. Chem. Chem. Phys. 2010, 12, 1543-1549.
16. M. Nirmal, L. Brus, Acc. Chem. Res. 1999, 32, 407-414.
17. T. Wang, S. S. Farvid, M. Abulikemu, P. V. Radovanovic, J. Am. Chem. Soc. 2010, 132, 9250-9252.
18. H. Zhou, W. Cai, L. Zhang, Appl. Phys. Lett. 1999, 75, 495-497.
19. A. Janotti, C. G. Van de Walle, Phys. Rev. B: Condens. Matter Mater. Phys. 2007, 76, 165202.
20. L. Schmidt-Mende, J. L. MacManus-Driscoll, Mater. Today (Oxford, U. K.) 2007, 10, 40-48.
21. H.-M. Xiong, Y. Xu, Q.-G. Ren, Y.-Y. Xia, J. Am. Chem. Soc. 2008, 130, 7522-7523.

22. X. Tang, E. S. G. Choo, L. Li, J. Ding, J. Xue, J. Chem. Mater. 2010, 22, 3383-3388.
23. H. Wang, L. Jia, P. Bogdanoff, S. Fiechter, H. Mohwald, D. Shchukin, Energy Environ. Sci. 2013, 6, 799-804.
24. M. W. Ahn, K. S. Park, J. H. Heo, J. G. Park, D. W. Kim, K. J. Choi, J. H. Lee, S. H. Hong, Appl. Phys. Lett. 2008, 93, 263103.
25. Z.-Y. Pan, J. Liang, Z.-Z. Zheng, H.-H. Wang, H.-M. Xiong, Contrast Media Mol. Imaging 2011, 6, 328-330.
26. Z.-Y. Zhang, Y.-D. Xu, Y.-Y. Ma, L.-L. Qiu, Y. Wang, J.-L. Kong, H.-M. Xiong, Angew. Chem., Int. Ed. 2013, 52, 4127-4131.
27. C. Zhang, J. Lin, Chem. Soc. Rev. 2012, *41*, 7938-7961.
28. X. Wu, G. Siu, C. Fu, H. Ong, Appl. Phys. Lett. 2001, 78, 2285-2287.
29. H. M. Xiong, D. G. Shchukin, H. Möhwald, Y. Xu, Y. Y. Xia, Angew. Chem., Int. Ed. 2009, 48, 2727-2731.
30. L.-W. Sun, H.-Q. Shi, W.-N. Li, H.-M. Xiao, S.-Y. Fu, X.-Z. Cao, Z.-X. Li, J. Mater. Chem. 2012, 22, 8221-8227.
31. H. L. Tuller, S. R. Bishop, Annu. Rev. Mater. Res. 2011, 41, 369-398.
32. I. Bilecka, M. Niederberger, Nanoscale 2010, 2, 1358-1374.
33. M. Baghbanzadeh, L. Carbone, P. D. Cozzoli, C. O. Kappe, Angew. Chem., Int. Ed. 2011, 50, 11312-11359.
34. B. L. Hayes, Microwave synthesis: chemistry at the speed of light. CEM Pub.: 2002.
35. K. H. Tam, C. K. Cheung, Y. H. Leung, A. B. Djurišić, C. C. Ling, C. D. Beling, S. Fung, W. M. Kwok, W. K. Chan, D. L. Phillips, L. Ding, W. K. Ge, J. Phys. Chem. B 2006, 110, 20865-20871.
36. S. Cho, J. Ma, Y. Kim, Y. Sun, G. K. Wong, J. B. Ketterson, Appl. Phys. Lett. 1999, 75, 2761-2763.
37. S. Monticone, R. Tufeu, A. Kanaev, J. Phys. Chem. B 1998, 102, 2854-2862.
38. K. Vanheusden, C. Seager, W. Warren, D. Tallant, J. Voigt, Appl. Phys. Lett. 1996, 68, 403.
39. A. Van Dijken, E. Meulenkamp, D. Vanmaekelbergh, A. Meijerink, J. Lumin. 2000, 90, 123-128.
40. A. J. Morfa, B. C. Gibson, M. Karg, T. J. Karle, A. D. Greentree, P. Mulvaney, S. Tomljenovic-Hanic, Nano Lett. 2012, 12, 949-954.
41. X. Chen, L. Liu, Y. Y. Peter, S. S. Mao, *Science* 2011, *331*, 746-750.
42. A. L. Schoenhalz, J. T. Arantes, A. Fazzio, G. M. Dalpian, J. Phys. Chem. C 2010, 114, 18293-18297.
43. N. J. Lawrence, J. R. Brewer, L. Wang, T.-S. Wu, J. Wells-Kingsbury, M. M. Ihrig, G. Wang, Y.-L. Soo, W.-N. Mei and C. L. Cheung, *Nano Lett.*, 2011, **11**, 2666-2671.
44. Y. Y. Tay, S. Li, C. Q. Sun, P. Chen, Appl. Phys. Lett. 2006, 88, 173118-173113.
45. P.-T. Hsieh, Y.-C. Chen, K.-S. Kao, C.-M. Wang, Appl. Phys. A: Mater. Sci. Process. 2008, 90, 317-321.
46. A. Kelly, G. W. Groves, P. Kidd, Crystallography and crystal defects, John Wiley & Sons, 2000. pp. 289.

